The rate and evenness of the substitutions on hyaluronan grafted by dodecanoic acid influenced by the mixed-solvent composition

Eva Kutálková[a], Josef Hrnčiřík[a], Roman Witasek[a], Marek Ingr[a,b,*], Gloria Huerta-Ángeles[c], Martina Hermannová[c], Vladimír Velebný[c]

[a]Tomas Bata University in Zlín, Faculty of Technology, Department of Physics and Materials Engineering, Nám. T.G. Masaryka 5555, 76001 Zlín, Czech Republic

[b]Charles University, Faculty of Science, Department of Biochemistry, Hlavova 8/2030, 12843 Praha 2, Czech Republic

[c] Contipro a.s., Dolní Dobrouč 401, 561 02 Dolní Dobrouč, Czech Republic

Abstract

In this work, low molecular weight (17 kDa) hyaluronan was modified by dodecanoyl substituents. The activation of dodecanoic acid was mediated by benzoyl chloride towards the preparation of a mixed anhydride, which reacts in a second step with HA in water mixed with an organic solvent. The effect of the cosolvent was studied and showed an even distribution of substituents and higher reaction rate in water:1,4-dioxane compared to water:tert-butanol where substituents occupy adjacent positions. The chemical characterization of the prepared derivatives was elucidated by NMR, FTIR spectroscopy, thermal analyses, and gas chromatography, while the distribution of substituents was evaluated by enzymatic degradation. Molecular-dynamics simulations reveal opposite solvent separations around HA and dodecanoyl chains, that is stronger in water:tert-butanol solution. The resulting incompatibility of solvation-shells of the two entities repels the reaction intermediates from the HA chain and drives them towards the already bound substituents, explaining the observed differences in the distribution evenness. Thus, the influence of the solvent on the reaction selectivity is observed by shielding reactive sites

around HA. Therefore, a control of the distribution of the substituents was obtained by defining the concentration of HA and used cosolvent.

Keywords:

Amphiphilic hyaluronan, mixed anhydrides, mixed solvent.

1. Introduction

Hyaluronan or hyaluronic acid (HA) is a naturally occurring polymer consisting of D-glucuronic acid (GlcA) and *N*-acetyl-D-glucosamine (GlcNAc) units linked by alternating β-(1→4)- and β-(1→3)- glycosidic bonds. Its highly hydrophilic nature, caused by the Gibbs-free-energy lowering by constituting the HA-water interactions on account of interactions between different parts of the HA chain, results in strong swelling of the HA random coils in aqueous environment. Numerous experimental works [1–3] described HA random coils along with the determination of their radii of gyration R_g, which corresponded with our previous molecular-dynamics (MD) study [4]. The tertiary structures of oligo HA and higher size chains are thermodynamically unstable in aqueous solution and are considered inexistent [5,6], although some authors declared their identification [7,8]. Intramolecular hydrogen bonds stabilize the semi-rigid nature of HA chains. Still, HA-water hydrogen bonds anchor the molecule to a well-structured solvation shell, protecting the molecule from intermolecular interactions [9]. Thus, HA is soluble in water, inert to interactions with other molecules and interacts with the binding sites of protein receptors (hyaladherins) [10].

The chemical modification of HA i.e. hydrophobization increases its shelf life and decrease its solubility in water. Hydrophobized high molecular weight HA has been used in ophthalmology [11,12], while low molecular weight modified HA is processed for drug delivery [13,14]. The hydrophobization of HA is usually performed in solvents such as dimethylsulfoxide (DMSO) or formamide for grafting long alkyl chain amines [15,16] or polymers to HA [17] and uses anhydrous conditions at high temperature. However, these conditions make the process expensive and are inconvenient for upscaling as HA had to be converted to either acid form or tetrabutylammonium salt (TBAHA) to become soluble in the organic solvent. This approach increases the chain fragmentation of HA, decreases the yield, and provides lower conversion due to harsh reaction conditions. For example, Wang and collaborators [18] reported the degradation of the molecular weight from 1.33×10^5 to 0.874×10^5 after the conversion to HATBA. Besides, Khetan and Burdick [19] mentioned that the purified yield of the modified HA was only 65% (based on moles) of HA present in the TBAHA. Lower yield was reported also by Zerobin et al. [20]. To overcome these problems, the chemical modification of HA is carried out in a mixture of organic solvents miscible with water, i.e. water:DMF [21], water:isopropanol [22] or water:DMSO [23]. These solvents may also bring some advantage for HA processing [24]. Despite the results of these studies, to our knowledge no systematic MD study of HA in any mixed water-organic solvent has been done yet.

A recent study shows the chemical HA modification by oleoyl residues using the mixed-anhydride method in water:1,4-dioxane and water:tert-butanol (2-methyl-2-propanol) mixed solvents [25]. The solvent composition influences not only the degree of substitution, but also the regioselectivity of the reaction. Therefore, this work was conducted to investigate the analogous esterification reaction with dodecanoyl residues to extend the versatility of the solvent-controlled approach for medium-length fatty acids. To the best of our knowledge

this is the first time MD simulations are performed with HA in mixed solvents to explain how the mixed-solvent composition controls the efficiency and evenness of the esterification reaction.

2. Materials and methods

2.1. Materials

Low molecular weight sodium hyaluronate (M_w = 17,000 g/mol, M_w/M_n = 1.50) was provided by Contipro a.s, Dolní Dobrouč, Czech Republic. The weight-average molecular weight (M_w) and polydispersity (M_w/M_n) were determined by SEC-MALLS before the chemical modification as described previously [26,27]. Dodecanoic acid (C12, ≥ 99.9 %), 4-(Dimethylamino)pyridine (DMAP, ≥99 %) and tert-butanol (99.9%) were obtained from Merck. Analytical grade CHROMASOLV® solvents were used for the chromatographic analysis. Deuterium oxide (D_2O), deuterated chloroform ($CDCl_3$) and DMSO-D6 were purchased from CortecNet (France). 1,4-dioxane (99 %), isopropanol (IPA, 99%), and sodium chloride (NaCl, 98%) were obtained from Lachner (Czech Republic). Benzoyl chloride (BC ≥ 99.0 %) was obtained from Sigma-Aldrich. Triethylamine (TEA, ≥ 99.0 %) were obtained from Penta, Czech Republic.

2.2. Synthesis of sodium dodecanoyl hyaluronate (HA-C12)

In the reaction flask, sodium hyaluronate (5g, 12.5 mmol) was dissolved in distilled water (50 mL). To that solution, 25 mL of the chosen organic solvent (tert-butanol or 1,4-dioxane) was slowly added. After the solution was homogeneous, TEA (3.8 mL, 37.5 mmol) and DMAP (0.076 g, 0.63 mmol) were added, then the mixture was stirred until a homogeneous solution was obtained. In a second flask, dodecanoic acid activation was carried out.

Dodecanoic acid (3.255 g, 16.3 mmol) was dissolved in 20 mL of the organic solvent used as in flask 1**.** After that, TEA (3.8 mL, 37.5 mmol) was added, followed by 2.28 g of benzoyl chloride (1.88 mL, 16.3 mmol). The formation of the mixed anhydride was carried out for 30 minutes at 25°C. Then, this solution was slowly poured to the flask containing HA. The flask 2 was washed out with 5 mL of the chosen organic solvent. The acylation reaction proceeded for two hours at room temperature under vigorous stirring. After two hours, the reaction was stopped by adding a saturated solution of NaCl. In the case of lower concentration (the described solution contains 5% (w/v) HA considering only HA and the mixed solvent – this quantification is used throughout the whole text) only the total volume of the reaction was multiplied (e.g. for 0.5% 10 times), keeping the molar equivalents of the reaction constant. The reaction product was precipitated with an excess of IPA (500 mL). The product was washed several times with solutions of IPA:water (85% v/v, 4 x 500 mL). Finally, the precipitate was washed two more times with 500 mL of IPA. The white powder was decanted, dried in an oven at 40°C for 24 hrs.

2.3. Determination of the degree of substitution by gas chromatography

The degree of substitution (DS_{GC}), i.e. the content of esters moieties (acyls), was measured by GC after alkaline hydrolysis of the sample as described recently [28]. The detailed description of the method is given in the Supplemetary information, section S4. The DS_{GC} means the extent of HA modification by hydrophobic side groups and is calculated according to the equation (1):

$$DS_{GC} = \frac{m_{FA,tot} - m_{FA,free}}{m_{sample}} \frac{M_{HA}}{M_{FA}} \times 100\% \qquad (1)$$

where $m_{FA,tot}$ is the amount of fatty acid determined in the derivative after alkaline hydrolysis, $m_{FA,free}$ is the amount of fatty acid unbound to HA chain, m_{sample} is the weight of

derivative, M_{HA} is molar mass of HA disaccharide (401 g/mol for sodium salt), and M_{FA} is molar mass of fatty acid.

2.4. Liquid chromatography coupled to mass spectrometry

Sample (3-5 mg) was dissolved in a mixture of 0.1M sodium phosphate buffer pH 5.0 and isopropanol (1:1, v/v) at the concentration 2 mg/mL. After complete dissolution, the sample was diluted with 0.1M sodium phosphate buffer to a final concentration of the derivative and isopropanol 1 mg mL^{-1} and 25 % (v/v), respectively. Then, to an aliquot (1 mL) a solution of hyaluronan lyase from *Streptococcus Pneumoniae* (SpHyl, 25 μL, approx. 6500 IU/mL) was added and incubated at 37°C for 2 h. The sample was diluted to 20 μg mL^{-1} with 30% methanol in water (v/v) and analyzed by LC-MS. An Acquity UPLC I-class chromatographic system connected to Synapt G2-Si mass spectrometer (Waters, Manchester, UK) was used for structural characterization of HA-C12. The separation was performed on Waters Acquity UPLC Protein BEH C4 column (1.7 μm, 300Å, 150×2.1 mm) at 40°C. The chromatographic eluent consisted of 0.1% formic acid in water and acetonitrile. Flow rate was set at 0.4 $mL \cdot min^{-1}$ and the following gradient of acetonitrile was applied: 0 min 30 %, 16.5 min 95 %, 17 min 95 %, 17.1 min 30 %. The injection volume was 5 μL.

The mass spectrometer was equipped with an electrospray ionization source operating in negative ion mode. Sodium formate (0.5 mmol L^{-1} in water/isopropanol = 10/90, v/v) was used for instrument calibration in the *m*/*z* range 50–1850. Instrumental parameters for C12-modified oligosaccharide analysis were set as follows (unless otherwise stated): spray capillary voltage 2.7 kV, source temperature 100 °C, sampling cone voltage 140 V, source offset 80 V, desolvation temperature 500 °C, cone gas flow (N_2) 50 L h^{-1}, desolvation gas flow (N_2) 850 L h^{-1}, nebulizer gas flow (N_2) 6.0 bar, trap collision voltage 4.0 V, transfer

collision voltage 2.0 V, trap gas flow (Ar) 2.0 mL min^{-1}, helium cell gas flow (He) 180.0 mL min^{-1}, ion mobility spectrometry gas (drift gas) flow (N_2) 90 mL min^{-1} and wave height 40.0 V. Ion mobility wave velocity was set at 500 m s^{-1}. Leucine enkephalin (200 ng mL^{-1}) at flow rate 5 μL min^{-1} was used as a lock mass. Mass chromatograms belonging to unsaturated di-, tri- and tetrasaccharides modified with 1, 2 and 3 acyl chains (*m/z* 939.3822 for $_{\Delta}$HA4-1×C12; *m/z* 1121.5492 for $_{\Delta}$HA4-2×C12; *m/z* 1303.7163 for $_{\Delta}$HA4-3×C12; *m/z* 560.2707 for $_{\Delta}$HA2-1×C12; *m/z* 736.3031 for $_{\Delta}$HA3-1×C12) were extracted and integrated. The extraction window was 0.02 amu. The percentage of each modified oligosaccharide in the mixture was calculated by equation (2).

$$w(\Delta HAx - i \times C12) = 100 \times \frac{A(\Delta HAx - i \times C12)}{\sum_{i=1}^{3} A(\Delta HAx - i \times C12)} \quad (2)$$

$w(_{\Delta}HAx\text{-}i\times C12)$ is the percentage of peak area belonging to one specific oligosaccharide in the sum of peak areas belonging to all other detected oligosaccharides. $_{\Delta}HAx$ can be $_{\Delta}$HA4, $_{\Delta}$HA2 and $_{\Delta}$HA3. The amount of other unsaturated modified oligosaccharides (mainly $_{\Delta}$HA2-1×C12, $_{\Delta}$HA3-1×C12) was low (≤ 5%). Therefore, they are included neither in the results section nor in eq. (2). Acquired data were processed with MassLynx 4.1 software (Waters, Milford, MA, USA).

2.5. Molecular-dynamics (MD) simulations

All MD simulations were carried out by NAMD 2.10 program package [29]. CHARMM 36 force field containing the parts for saccharide molecules [30] and fatty acids [31] was used for the both HA molecule and the saturated aliphatic chains, CGenFF topology and parameter files were used for the 1,4-dioxane and tert-butanol molecules, TIP3P model of water was applied. The force field of N-dodecanoyl-4-(dimethylamino)-pyridinium cation

168 (C_{12}-$DMAP^+$) and triethylammonium (TEA^+) ions were constructed using CHARMM-GUI
169 Ligand Reader & Modeler [32]. This instrument was also used to obtain the ester-bond
170 parameters between HA (C6 carbon of GlcNAc) and the 12-carbon aliphatic sidechain (C_{12}),
171 while the topology of this link was adopted from an analogously acetylated HA molecule
172 constructed by the CHARMM-GUI Glycan Modeler [33] (none part of the CHARMM-GUI
173 package can process the whole substituted HA molecule). Two configurations of substituted
174 HA molecules were considered – with the substituent at the end or in the middle of the chain,
175 i.e. on the GlcNAc residue number 1 or 11 (out of 20 residues), respectively, from the non-
176 reducing end. Formulas of all the simulated molecules are given in **Fig. S11**.

177 The preparation of the simulated systems started by the equilibration of the boxes of pure
178 mixed solvent. HA was then wrapped by these boxes to form the complete simulation box
179 of about 100Å edge. The energy of each system was minimized for 5400 fs prior to the MD
180 simulation. Integration was performed by the Verlet-I/r-RESPA MTS method with the slow-
181 force mollification, a timestep of 1 fs for bonding and 2 fs for non-bonding interactions and
182 10Å cutoff of non-bonding interactions was used. Full electrostatic calculations were
183 performed every 6^{th} fs using the Particle Mesh Ewald (PME) method. Simulations were
184 carried out in NPT system at the constant pressure of 1 atm and selected temperature for 200
185 ns. The pressure was controlled using the Langevin piston Nosé-Hoover method and the
186 temperature was controlled using Langevin dynamics.

187 HA oligosaccharides of 20 monosaccharide units were simulated in 7 different media: pure
188 water and three compositions of water:1,4-dioxane and water:tert-butanol solutions. In both
189 cases, the volume to volume ratios were defined as 2:1, 1:1 and 1:2 (organic-component
190 volume fractions 0.33, 0.50, 0.67), at 310 K and 277 K. Every simulation contains 10 Na^+
191 ions compensating the negative charge of HA. Other HA-oligosaccharides simulations were
192 performed in the presence of 5 C_{12}-$DMAP^+$ and 5 TEA^+ ions in the mixed solvents of

193 water:1,4-dioxane and water:tert-butanol of organic-component volume fraction 0.5 at 277
194 K and 310 K. C_{12}-substituted HA oligosaccharides were simulated in the presence of either
195 10 Na^+ or 10 C_{12}-$DMAP^+$ ions at 298 K in both solvents. For composition details of the
196 systems see **Table S3**.

197 The simulation results were visualized, and specific analyses, especially the determinations
198 of radial distribution functions (RDFs), were carried out using the VMD program [34]. The
199 number of atoms of a given molecule within a distance of 4 Å from a selected entity, HA or
200 the aliphatic chain, hereinafter called number of close atoms, was evaluated as a descriptor
201 of the closest part of the solvation shell of the entity. In case of the C_{12}-$DMAP^+$ reactants
202 number of whole molecules having at least one atom in equally defined area was evaluated
203 (hereinafter called number of close molecules). The output quantities were averaged within
204 the equilibrated time interval 50-200 ns and the standard deviations of the mean were
205 determined (for all the quantities it is lower than the symbols, therefore it is not shown in
206 the graphs).

207

208 ## 3. Results

209 ### 3.1. Synthesis of dodecanoic acid grafted to hyaluronan (HA-C12)

210 The activation of dodecanoic acid is mediated by benzoyl chloride (BC) and yields a
211 mixed aliphatic-aromatic anhydride in organic solvents miscible with water, i.e.,
212 tetrahydrofuran, 1,4-dioxane, isopropyl alcohol or tert-butanol. The mixed anhydride reacts
213 in the next step with the hydroxyl moieties of HA, yielding esterified HA (**Scheme 1**).
214 However, the solvent mixture drastically influences the selectivity of the reaction towards
215 the substitution at the primary and/or secondary hydroxyl moieties. While HA acylation

carried out in DMSO was reported to be more selective for short fatty acids [35], the selectivity for medium fatty acids is still unknown.

Several factors influence the degree of chemical modification and the distribution of substituents: polarity of the reaction media, the molar ratio of reagents, and the hydrophobicity of the fatty acid (ligand), the M_w of HA used for the chemical modification and the concentration of the reaction feed components.

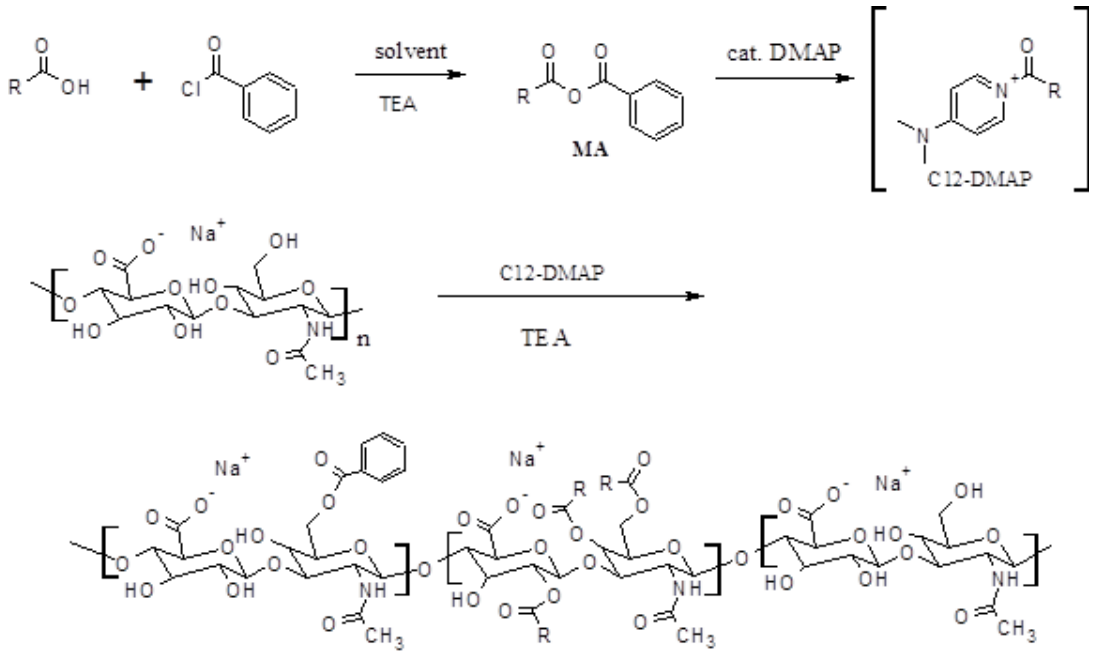

Scheme 1. *The esterification of HA by the mixed anhydride method is mediated by 4-dimethylamino pyridine and carried out in a mixed water:organic solvent system. R = -$C_{11}H_{23}$ (undecanoyl).*

Even though water-insoluble high molecular weight dodecanoyl derivatives of hyaluronan can be used to prepare thin films [36]. It is necessary to develop water-soluble derivatives for drug delivery [37]. It is worth mentioning that the structural characterization of derivatives is preferred by using low molecular weight HA due to the higher reaction efficiency and solubility of the conjugates. The results showed that the polymer concentration in the reaction feed drastically changes the conjugate's solubility probably due

to self-aggregation (**Table 1)**. The derivatives prepared at low concentration (0.5-1.5 % of HA in the reaction feed) were fully water soluble (lower turbidity and higher transmittance, $T \geq 65\%$). Contrary, the derivatives prepared at higher concentration (2.5-5%) produced highly viscous solutions or were insoluble in water due to the uneven substitution.

Fig. 1 depicts the ^{1}H NMR spectrum of HA-C12 recorded in NaOD (see the methodical description in section S1). NaOD was added to the sample, mixed and the spectra were acquired immediately to avoid the possible hydrolysis of HA, but the spectral resolution was strongly improved due to the *in situ* hydrolysis of substituents. On the contrary, the ^{1}H NMR spectrum of HA-C12 recorded in D_2O derivatives presented a broadening of the signals due to self-aggregation (see **Figs. S1, S2**). The degrees of substitution measured in NaOD and determined by NMR are in a good agreement with the ones determined by gas chromatography (Fig. 1.). All the spectra show typical proton chemical shifts of HA involving signal at 2.0 ppm belonging to -$NCOCH_3$ group, skeletal signals at 3.4–3.9 and anomeric resonances at 4.4–4.6 ppm. The ^{13}C-DEPT-HSQC NMR shows the remaining signals at 0.8, 1.3, 1.6 and 2.4 ppm, which were attributed to CH_3, and CH_2 (**Fig. S3**). Furthermore, the signals located at 7.6 (triplet), 7.5 (triplet) and at 7.9 (doublet of doublets) ppm, respectively reveal the benzoylation of hyaluronan. The signals located at 3.7 and 3.9 corresponding to the methylene protons C6 (GlcNAc) deshielded to 4.2 and 4.5 ppm in D_2O, respectively due to the esterification. Interestingly, the signals corresponding to the diasterotopic methylene protons in position C6, upfield to 2.78 and 3.11 ppm in NaOD. Several signals in HA backbone become double due to the esterification, but they were overlapped. Therefore, the enzymatic fragmentation of HA-C12 reveals the substitution positions (**section 3.2**).

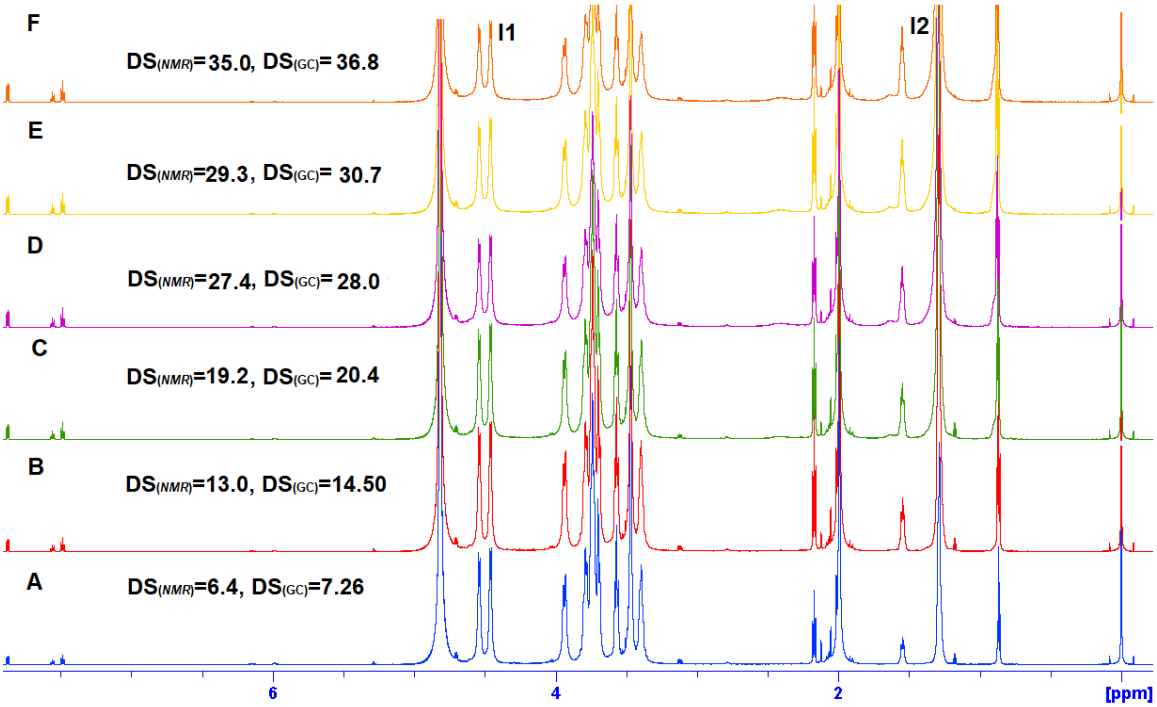

Fig. 1. *^{1}H NMR of HA-C12 measured in NaOD. DS values are in %.*

The formation of a covalent bond between dodecanoic acid and HA was further established by diffusion ordered NMR spectroscopy (DOSY) as depicted in **Fig. 2a**. The signals coming from the same molecule have the same diffusion coefficient. Because of the marked difference between the diffusion coefficients of the low molecular weight dodecanoic acid and HA, the DOSY map could easily establish the presence of non-attached fatty acid groups to HA, which obviously diffuse much faster than the bound acyl groups as compared to free dodecanoic acid (**Fig. 2b**). DOSY experiment showed similar diffusion behaviour for all signals (except for residual isopropanol and the standard of (trimethylsilyl)propionic-2,2,3,3-d4 acid sodium salt, which presented a higher diffusion), thus, indicated that all of the proton resonances in this region belonged to one structural complex (HA-C12).

The dodecanoyl moieties present the same diffusion behaviour as HA (which confirmed the formation of a covalent bond between the fatty acid and HA. In addition, it

can be well recognized that the diffusion of the methyl substituent of C12, which is located at 0.8 ppm presented even a slower diffusion (i.e. the signal is placed at larger –log D values along y axis). The restricted mobility in D_2O is explained by self-aggregation of the conjugate.

The aggregation phenomenon was confirmed acquiring DOSY in D_2O with 0.9% (w/v) of NaCl. The kosmotropic salt made all the molecule appear even "larger" due to slower diffusion, similar to reported earlier [38]. This means that there is aggregation between the hydrophobic acyl substituents that it is leading to slower diffusion. Furthermore, the critical aggregation concentration (CAC) for the derivative (HA-C12) confirmed the self-aggregation. CAC was determined by Nile red encapsulation and was found to be ~ 0.02 mg/mL (**section S2**, **Fig. S4**).

The formation of the ester bond was further evidenced by infrared spectroscopy (**section S3**). The esterification was confirmed by the peak at 1729 cm^{-1}, as reported earlier (Huerta-Ángeles et al., 2020). The signals at 2924 and 2835 cm^{-1} corresponded to the asymmetric and symmetric vibrations of *C-H* due to the presence of the alkyl moiety as substituent, which were more prominent compared to HA used for chemical modification (**Fig S5**).

Furthermore, the purity of the samples was determined by GC (**section S4**) and thermal analyses (**Table S2**). The purity was given by the absence of free dodecanoic and benzoic acids (**Fig. S6**), and determination of ash and dry matter (**Fig. S7-S9**).

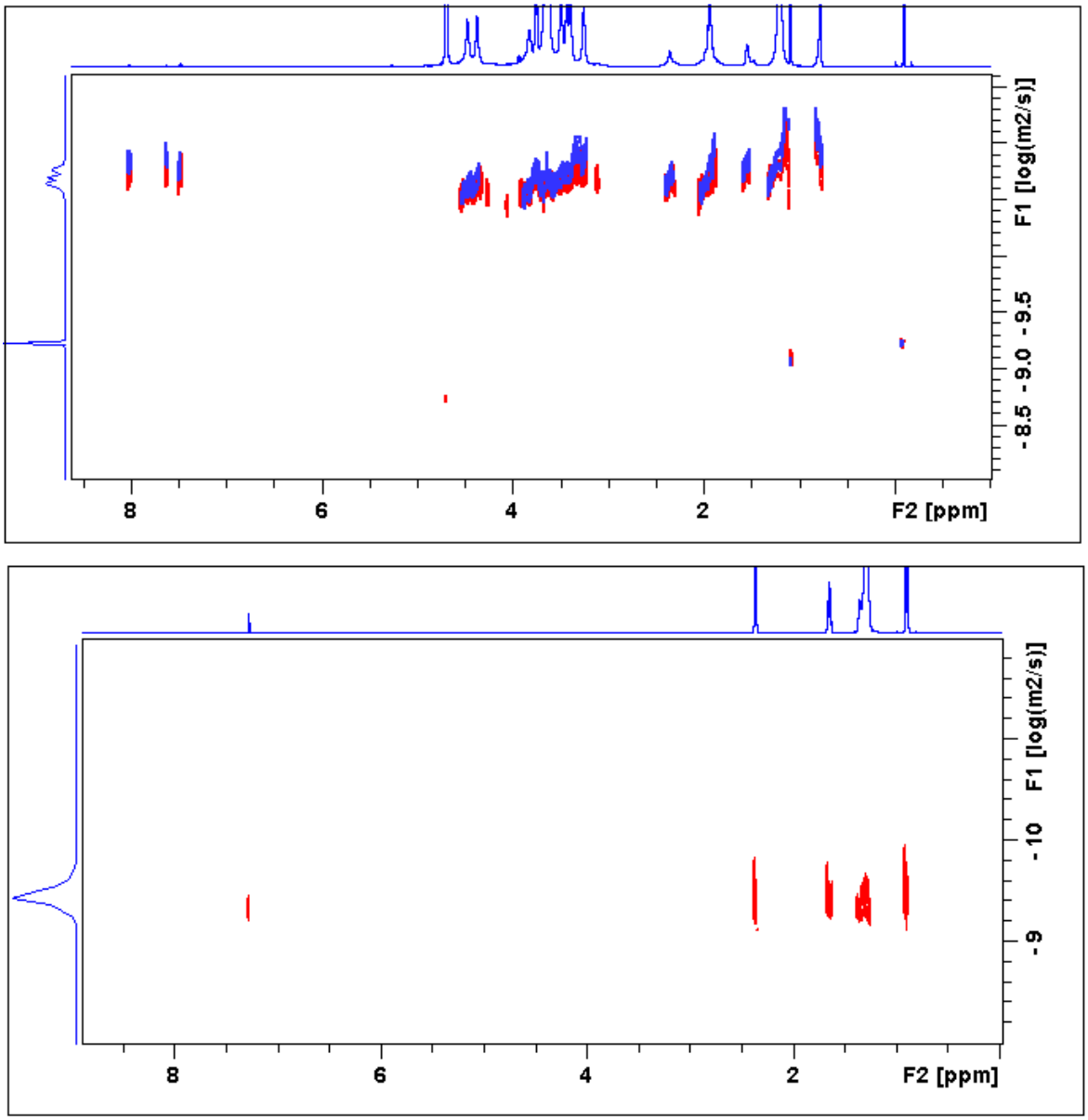

Fig. 2*. (**a**) DOSY NMR of HA-C12 measured in D_2O (red) and blue (0.9% NaCl) corresponding to sample* ***Table 1****, entry 6. (**b**) Lauric acid measured in $CDCl_3$*

Table 1. Effect of the concentration of HA on the synthesis of HA-C12 in 1,4-dioxane or tert-butanol. The esterification reaction was performed using LMW-HA (17,000 g/mol) and 1.3 eq. of activated dodecanoic acid for 2 hours at 25°C.

Entry	Conc. HA[a] (g/L)	DS_{GC}[b] (%)	NTU[c]	T (%) [d]
1,4-dioxane				
1	5	7.1±0.01	1.1±0.05	99.6±0.003
2	10	14.5±0.02	1.3±0.07	99.2±0.019
3	15	20.4±0.02	1.7±0.52	99.4±0.003
4	25	28.0±0.1	20.3±0.32	64.4±0.015
5	30	30.7±0.2	48.4±0.28	37.6±0.069
6	50	36.8±0.4	82.1±1.02	24.7±0.032
tert-butanol				
7	5	7.4±0.1	0.7±0.05	95.4±0.003
8	25	20.9±0.2	2.2±0.13	93.3±0.003
9	50	9.8±0.1	2.7±0.04	94.4±0.003

[a]Concentration of HA used for the chemical modification (w/v)
[b]DS_{GC} is the average of three independent determinations
[c]NTU stands for nephelometric turbidity, see section S5.
[d]Transmittance was determined by UV-Vis at 660 nm in 1% (w/v) solution.

Even though it is expected that the esterification reactions tend not to reach completion, **Table 1** shows that 1,4-dioxane was able to produce ~30% conversion at high concentration of HA. Contrary, the conversion of HA to HA-C12 in alcohols (tert-butanol) was not efficient. Esterifying multiple hydroxyls on a disaccharide provides an additional challenge due to steric hindrance between neighboring alkyl moieties.

3.2. Enzymatic degradation for the determination of the distribution of substituents

315 The solubility of the derivative can be explained in terms of even distribution of the
316 synthesized derivatives. Unsaturated C12-modified tetrasaccharides (ΔHA4-1×C12, ΔHA4-
317 2×C12, ΔHA4-3×C12) are the main SpHyl degradation products of HA-C12 prepared in
318 both 1,4-dioxane and tert-butanol. Extracted ion chromatograms of stated species present in
319 HA-C12 prepared in 1,4-dioxane or tert-butanol are shown in **Fig. S10**. The amount of
320 ΔHA4-1×C12 decreases while ΔHA4-2×C12 and ΔHA4-3×C12 increase with increasing
321 DS (**Fig. 3**). At similar DS, the reactions carried out in tert-butanol showed a high percentage
322 of di- and trisubstituted tetrasaccharides. Interestingly, the substitution predominantly takes
323 place at C4 and C6 of one GlcNAc, which can be only observed after enzymatic degradation.
324 The derivative containing a higher amount of ΔHA4-1×C12 had an even distribution of acyl
325 chains and is more soluble in water. Notably, the combination of 1,4-dioxane and diluted
326 conditions produced these derivatives.

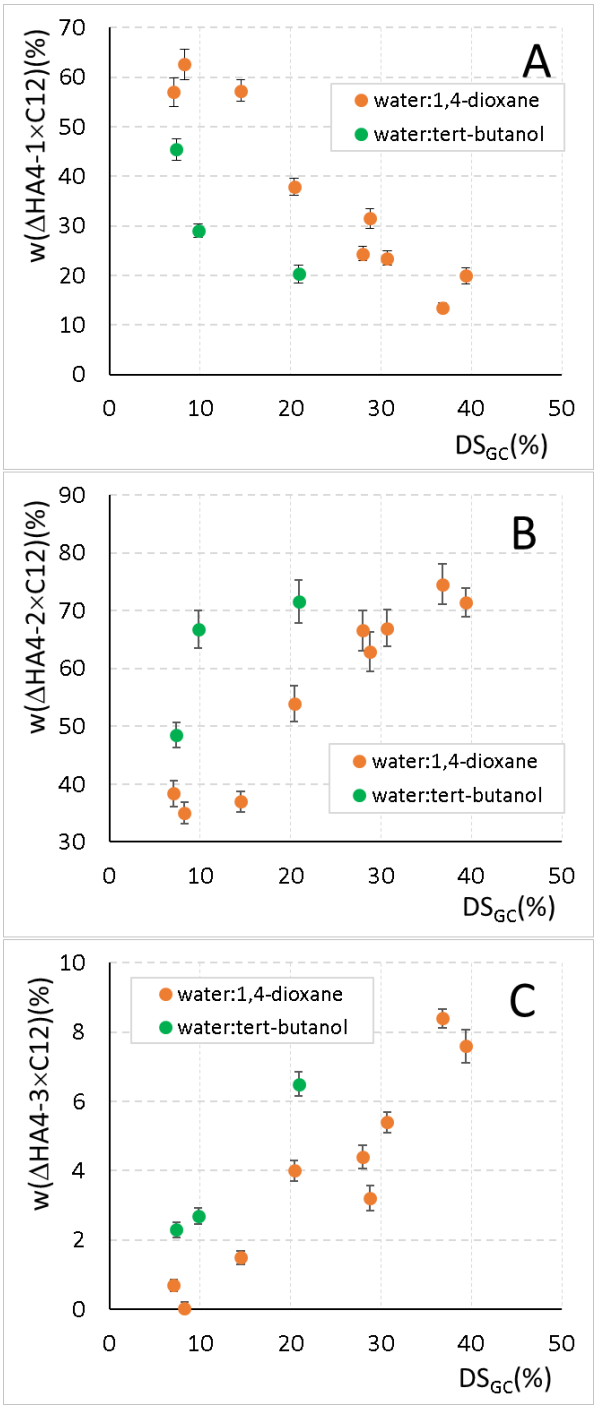

Fig. 3*. The amounts of mono- (A), di- (B) or trisubstituted (C) unsaturated tetrasaccharides plotted against DSGC. Derivatives prepared in 1,4-dioxane and tert-butanol are showed in orange and green, respectively. The esterification reaction was performed using HA (17,000 g/mol) and 1.3 eq of activated C12 for 2 hours at 25°C.*

3.3. Separation of solvent components around the free and substituted HA oligosaccharides

In order to explain the different properties of the substitution reaction in the different mixed solvents, 200ns MD simulations of both free and C12-monosubstituted HA chains of 20 monosaccharide units were simulated in both kinds of the mixed solvents of the organic-component volume fraction of 0.5. Equilibration of these simulations is demonstrated by the stable values of the numbers of close atoms of individual solvent components (for definition see section 2.5.) from the whole molecules and from the substituents (**Fig. S12**) and also of the interaction energies between the aliphatic sidechain and the solvent components (**Fig. S13**). Simulations of non-substituted HA molecules were carried out also at the temperatures of 277 K and 310 K and for the organic-component volume fractions of 0.33, 0.5 and 0.66. The RDFs for the volume fraction of 0.5 are shown in **Fig. 4** and show a strong solvent separation in the vicinity of the HA chain reaching the distance of about 25 Å.

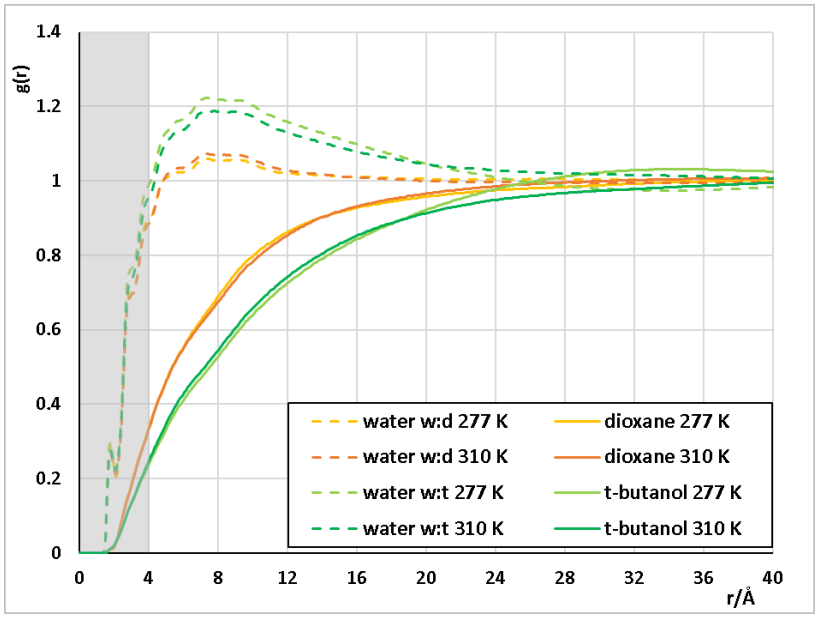

Fig. 4. *RDFs of the solvent components of the 50% (v/v) mixed solvents water:1,4-dioxane (denoted w:d) and water:tert-butanol (w:t) for 277 K and 310 K.*

In both the mixed solvents the HA solvation shell is enriched by water and deprived of the organic component relative to the bulk solvent. Obviously, the separation is remarkably stronger in the water:tert-butanol mixture (see a simulation snapshot in **Fig. S14**), where the maximum water concentration, occurring at the distance of 8 Å, is about 1.2 higher than the bulk concentration compared to the value of about 1.06 for water:1,4-dioxane. Simultaneously, analogous ratios for the organic component in the same distance are 0.52 and 0.68, respectively. Interestingly, the temperature dependence of the solvent separation is low and is slightly stronger at 277 K. A comparison of the close-atoms numbers of the solvent components (**Fig. S15**) shows that the solvent separations are consistent throughout the studied composition range. Moreover, the strong attractive interaction between HA and water is also supported by the quadratic dependence, with higher slope for water:tert-butanol, of relative enrichment of the close solvation shell by water calculated as the ratio of the close-atoms number and its projected bulk value (**Fig. S16**).

As the solvent separation around the free HA molecules showed a small temperature dependence, the simulation of substituted HA was carried out at 298 K. The radial distribution functions (RDFs) of the individual solvent components around the HA chain are shown in **Fig. 5** for the substituent located in the middle of the HA chain.

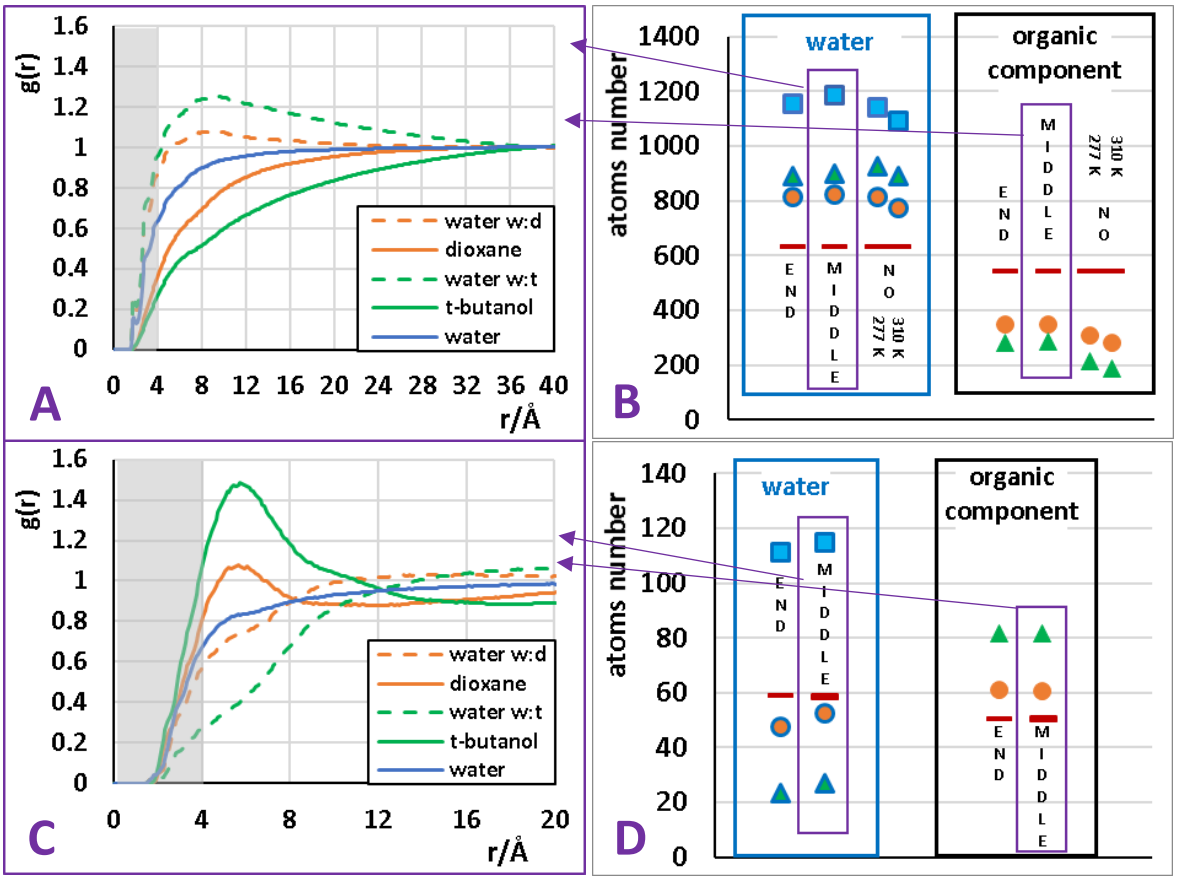

Fig. 5. *RDFs of the solvent components in the 50% (v/v) mixed solvents water:1,4-dioxane (orange) and water:tert-butanol (green) and pure water (blue) around the C_{12}-substituted HA molecules. A: RDFs at the HA chain itself for 298 K and substituent in the middle. B: Numbers of close atoms (within the 4Å distance from HA, indicated by the grey background in panel A) of water (left) and organic component (right) for both substituent positions and free HA molecules (simulated at different temperatures). Violet frames and arrows indicate the system shown in panel A. C and D: Same as A and B, but for the substituent instead of HA chain.*

Obviously, the solvent distribution around HA is very similar to that at the free HA chains. The numbers of close atoms in **Fig. 5B** indicate a negligible dependence of the HA solvation-shell structure on the substituent position, at the end or in the middle of the chain.

Analogously, RDFs of the solvent components around the substituent, i.e. the C_{12} aliphatic sidechain, were evaluated (**Fig. 5C**, position in the middle of HA chain, 298 K). They show a completely opposite solvent separation than at the HA chain. The solvation shell of the sidechain is strongly deprived of water and enriched by the organic component whose concentration reaches its maximum at about 6 Å from the sidechain and then relaxes towards its bulk value reaching it approx. at 12 Å.

In water:tert-butanol mixture the solvent separation is remarkably stronger than in water:1,4-dioxane. The ratios of the water and organic-component close atoms numbers at the sidechain (**Fig. 5D**) are 3.3 and 1.2, respectively (bulk solvent value 0.86), again almost independently of the substituent position. In addition, the RDFs in **Fig. S17B** show that the concentration maximum of tert-butanol methyl-carbon atoms is closer to the aliphatic sidechain than that of the oxygen atoms by approx. 1.5 Å which agrees with the distance of these atoms in the tert-butanol molecule. The amphiphilic character of tert-butanol molecules thus causes their strong preferential orientation by the methyl groups towards the aliphatic sidechain, while at the HA chain no such orientation takes place (**Fig. S17A**). On the contrary, RDFs for 1,4-dioxane carbon and oxygen atoms show significant difference neither at HA nor at the aliphatic sidechain (**Fig. S17**) indicating the random orientation of these molecules.

Similar solvent separation was observed also around the aliphatic chain of the C_{12}-$DMAP^+$ reactant – see the comparison with the sidechain bound on HA in **Fig. S18**. The small differences of the distribution functions are caused rather by the different surroundings of the C_{12} chain in the two cases that necessarily influences the RDFs at the longer distances.

3.4. Separation of solvent components around the free and substituted HA oligosaccharides

Free and C_{12}-substituted HA oligosaccharides were simulated in the presence of the reaction intermediates (C_{12}-$DMAP^+$) to evaluate the influence of the mixed solvents on the course of the esterification. The free HA chains were simulated together with 5 C_{12}-$DMAP^+$ molecules. Furthermore, 5 TEA^+ molecules were added to make the environment closer to the experimental conditions. The simulation was carried out in 50% (v/v) mixed solvents at 277 K and 310 K.

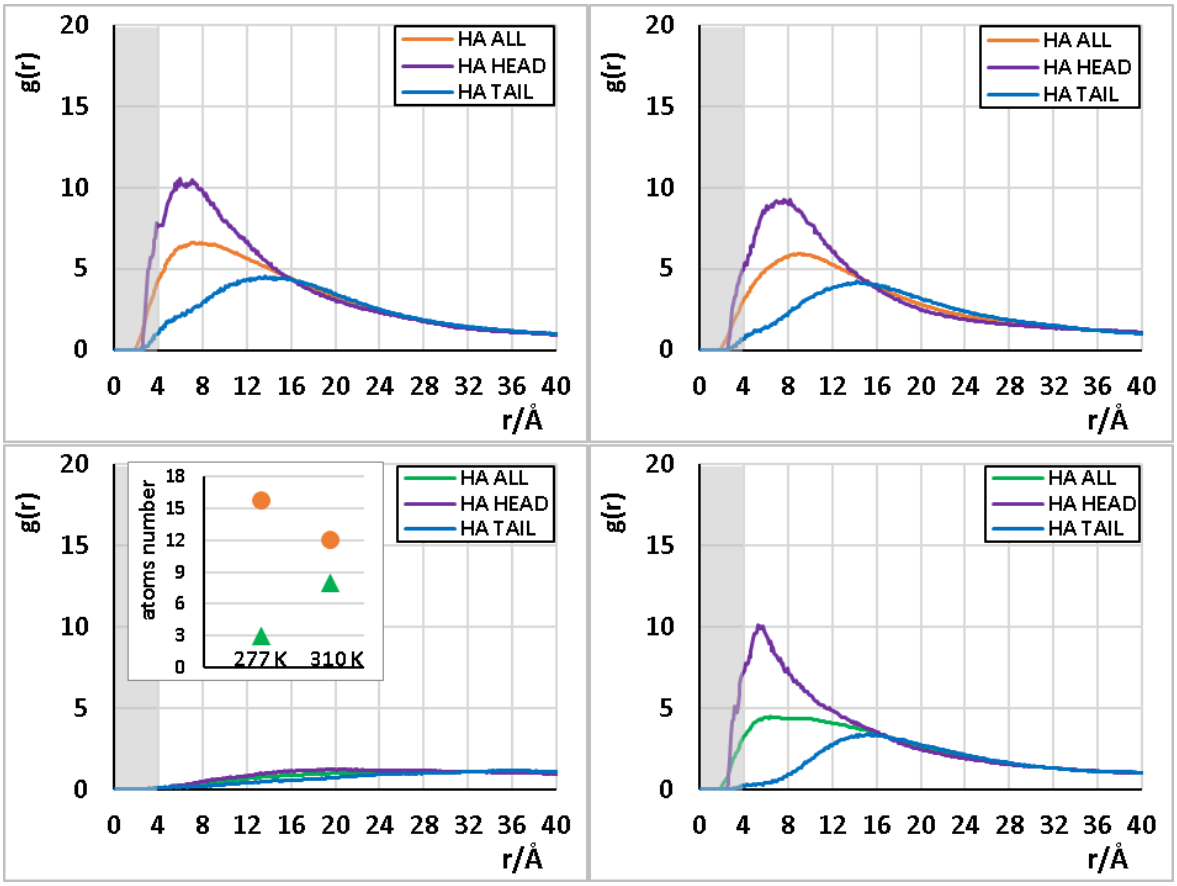

Fig. 6. *RDFs of C_{12}-$DMAP^+$ around HA molecules at 277 K (left) and 310 K (right) for water:1,4-dioxane (up) and water:tert:butanol (down) for the whole molecule, the head (carbon atoms of the DMAP heterocycle) and tail (last five carbon atoms of the sidechain). Inset – numbers of close atoms of C_{12}-$DMAP^+$ at HA within the region indicated in grey.*

RDFs in **Fig. 6** show an essential difference between the two mixed solvents. In water:1,4-dioxane the distributions are almost independent of temperature, only in the closest area the number of C_{12}-DMAP$^+$ atoms is somewhat higher (**Fig. 6**, inset) at the lower temperature indicating the disturbance of the attractive interaction by the thermal motion. This indicates an essentially enthalpic stabilization of C_{12}-DMAP$^+$ at HA by the electrostatic interaction between the positive and negative charges of C_{12}-DMAP$^+$ and HA, respectively. In water:tert-butanol, on the contrary, the occurrence of C_{12}-DMAP$^+$ in the HA vicinity is very rare at 277 K while at 310 K it grows substantially indicating an entropy-based stabilization of this state. It indicates that in this solvent the approach of C_{12}-DMAP$^+$ to HA requires a certain restructuring of the solvation shells of HA and C_{12}-DMAP$^+$ supported by the higher temperature. Its deeper understanding, however, needs more targeted MD simulations and will be a matter of further research.

3.5. Interactions of the reaction intermediates with substituted HA oligosaccharides

Substituted HA chains were simulated in both 50% (v/v) mixed solutions in the presence of 10 C_{12}-DMAP$^+$ molecules at 298 K. The C_{12}-DMAP$^+$ distributions around HA and the sidechain are well equilibrated within the 200ns simulations – see the time development of the numbers of close C_{12}-DMAP$^+$ molecules in **Fig. S19**.

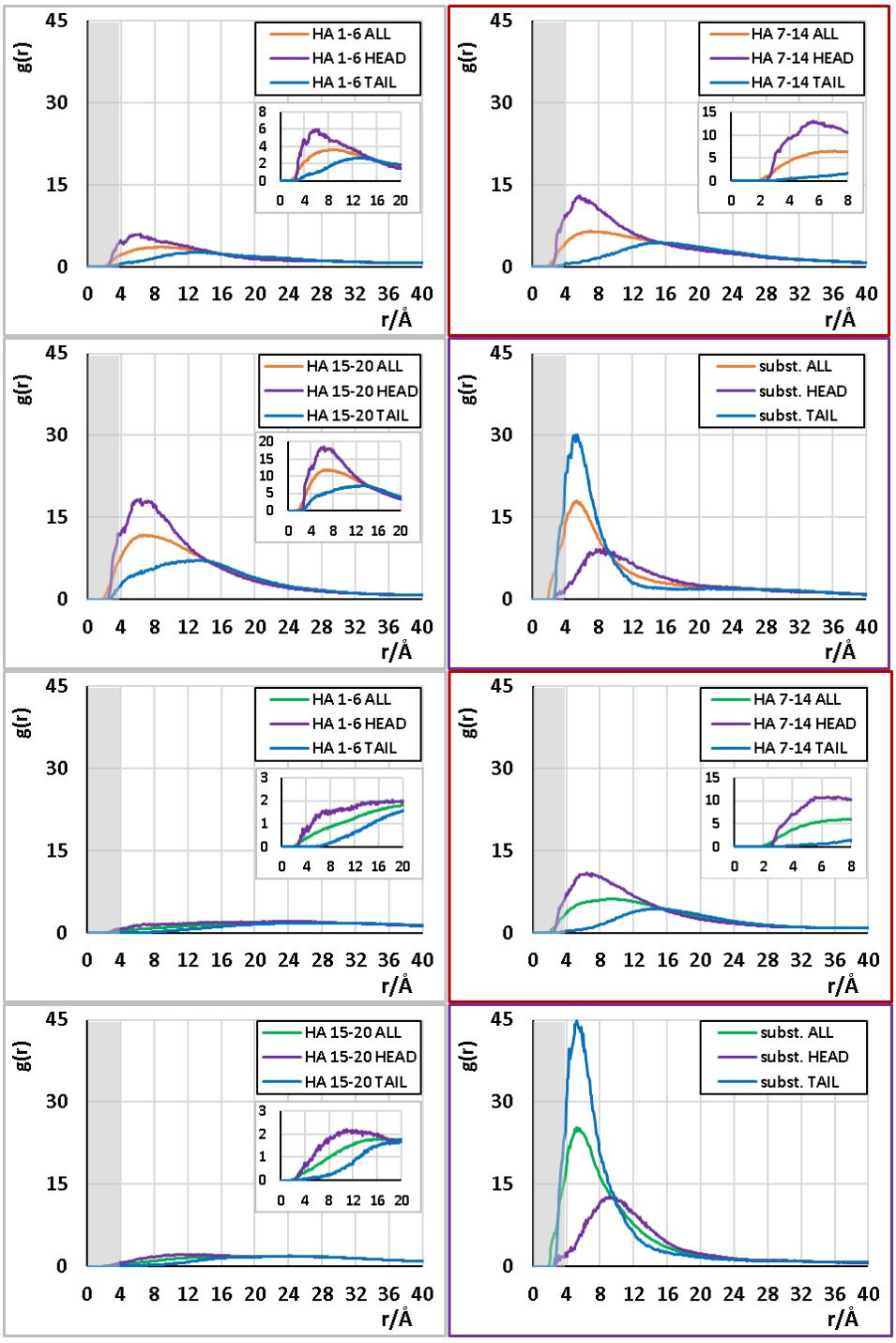

Fig. *7. RDFs of the C_{12}-DMAP$^+$ molecules, 50% (v/v) water:1,4-dioxane (upper quartet) and water:tert-butanol (lower quartet), 298 K , for individual parts of the HA molecule substituted in the middle of the chain. In every quartet, grey-framed plots are related to the end parts of the HA chain (residues 1-6 and 15-20), red-framed to the central part of HA (residues 7-14) bearing the substituent and violet-framed to the substituent itself. For better*

comparability, all graphs have equal scales, details of the closer parts of the RDFs are shown in the insets.

RDFs of the C_{12}-$DMAP^+$ molecules were calculated separately around individual "thirds" of the HA chain containing first 6, middle 8 and last 6 monosaccharide residues (**Fig. 7**) as well as around the substituent itself. In water:1,4-dioxane the situation at individual parts of HA is practically equal and independent of the substituent position. The C_{12}-$DMAP^+$ molecules are rather strongly electrostatically attracted to the HA chain which not only increases their concentration at HA, but also causes the preferential orientation with the positively charged head ($DMAP^+$ moiety) towards this molecule – see the RDFs of head and tail (last 5 carbons of the aliphatic chain) atoms in **Fig. 7**. On the contrary, in water:tert-butanol the C_{12}-$DMAP^+$ molecules are far less attracted to HA in the substituent-free parts of the molecule, consistently with the non-substituted HA chains. Close to the substituent, however, the number of C_{12}-$DMAP^+$ is remarkably higher. It indicates that the aliphatic sidechain disturbs the water-rich solvation shell of HA, being itself wrapped by tert-butanol molecules, and thus allows C_{12}-$DMAP^+$ to approach the HA chain. This phenomenon is more pronounced for the substituent located in the middle of the HA chain, since at the end (**Fig. S20**) the aliphatic chain may stick aside of the HA chain diminishing thus its positive effect on the reactants approach.

4. Discussion

The promising potential of the mixed solvents to control the degree of substitution of the esterification of HA, as well as the distribution of the substituents along the chain, was shown recently on the case of oleoyl residues [25]. To investigate the universality of these findings, esterification of HA by dodecanoyl residues was carried out by the same

methodology in the same mixed solvents, water:1,4-dioxane and water:tert-butanol in the volume ratio 1:1. The observed trends reproduced those of the previous study. Remarkably higher degree of substitution was reached in water:1,4-dioxane as well as its growth along with the concentration of the reactants in the reaction feed. While in water:1,4-dioxane the distribution of the substituents was relatively even, in water:tert-butanol clustering of the substituents, resulting in more frequent occurrence of multiply substituted oligosaccharides after cleaving HA enzymatically, was observed. The agreement of both these studies indicates that the influence of the mixed solvents on the reaction course is general for various kinds of non-polar aliphatic substituents. The solvent composition affects especially the approach of the reactants to the HA chain. An investigation of this phenomenon was based on MD simulations of non-substituted and substituted HA molecules both in pure mixed solvents and in the presence of the reaction intermediates.

MD simulations were carried out for 200 ns and this time was sufficient for the equilibration of all the distributions of molecules as well as the interaction energies (**Figs. S12, S13, S19**) since the systems only contain small molecules without internal motions with high energetic barriers. Compared to water:1,4-dioxane solution, water:tert-butanol mixture is more prone to solvent separation at both the hydrophilic HA molecule and the aliphatic sidechain (**Fig. 4, 5**). In the vicinity of HA both the organic components are repelled from the solvation shell, but they differ in the intensity of the effect and in the radius of the zone where the solvent composition differs from the bulk value. For instance, if the bulk ratio the organic to water atoms is 1, in the closest area it is only about 0,30 for tert-butanol and 0,43 for 1,4-dioxane and in the point of maximum water concentration 0,44 and 0,70, respectively. Hence, the solvation shell in water:tert-butanol is enriched by water remarkably more than in water:1,4-dioxane. Moreover, the radius of the water-enriched zone is much wider for tert-butanol reaching the bulk value at approx. 34 Å in contrast to 24 Å. If the

488 solvation shell is considered as a cylinder wrapping the HA molecule, the simulated HA
489 molecule repels approx. 170 tert-butanol- and attracts 700 water molecules, while for the
490 water:1,4-dioxane solution these numbers are only 50 and 240, respectively. On the contrary,
491 the solvation shell of the aliphatic sidechain of the substituted HA molecule is enriched by
492 the less polar organic component (**Fig. 5**). Although the long-distance parts of the
493 distribution functions are biased by the reverse solvent separation around HA, the ratios of
494 the numbers of close atoms of the organic component and water – 3.3 for water:tert-butanol,
495 1.2 for water:1,4-dioxane, 0.86 for bulk – support the apparent fact of stronger solvent
496 separation in water:tert-butanol. Amphiphilic tert-butanol molecules are uniquely oriented
497 by their methyl groups towards the aliphatic chain by hydrophobic interactions.
498 Accordingly, this mixture is also more prone to components micro-separation (**Fig. S21)**
499 reported previously by [39].

500 As shown in **Table 1**, the reaction rate, and thus also the DS, initially grows with the
501 concentration of both the reactants, HA and the activated dodecanoic acid, in accord with
502 the standard kinetic control. It was, however, shown that it is only valid below the coil
503 overlap point of the polymer. This point was reported to be at concentration ~ 0.86 wt.% for
504 LMW-HA (MW≥ 37,000 g/mol) in water [40,41]. As the HA chains fill the solution, the
505 reaction rate is affected by steric effect of the coils (at concentration ≥ 0.86 wt.%). Moreover,
506 the viscosity of the reaction mixture influences the rate of reaction, as well as the solubility
507 of the mixed anhydride. In the mixed solvents the separation of their components may further
508 contribute to the decrease of the reaction efficiency observed especially in water:tert-butanol
509 above the HA concentration of 25 g/l in the reaction feed. Considering the solvation shell as
510 a cylinder of a mean radius of 35 Å inferred from MD, its formally calculated volume at the
511 HA concentration of 25 g/l is about 1.4-times higher than the whole volume of the solution.
512 This situation likely leads to concentration of HA in water-rich zones while C_{12}-$DMAP^+$

remains in the tert-butanol enriched areas having thus limited access to HA. In water:1,4-dioxane this effect plays only a minor role since the solvation shell is narrower and the solvent separation weaker, which makes the rate decrease rather small.

MD simulations show that for the C_{12}-DMAP$^+$ reactants, even at low HA concentration, it is more difficult to approach HA in water:tert-butanol solution. It is, therefore, not surprising that the efficiency of the reaction measured by DS is lower here than in water:1,4-dioxane. At 298 K, the occurrence of the C_{12}-DMAP$^+$ head in the close area at HA in the latter solvent is, in average, about 3-4 times lower which roughly corresponds with the observed difference in DS. Although the temperature dependence of the reaction efficiency was not investigated experimentally, it can be expected that in water:1,4-dioxane the temperature effect will not be strong. With the temperature growth the number of reactant molecules attacking HA slightly decreases which may, on the other hand, be compensated by a higher rate of the reaction step itself. In water:tert-butanol, however, the number of reactants approaching HA grows quite rapidly with the temperature (**Fig. 6**) which could lead to the overall reaction-rate increase.

The evenness of the substituent distribution on the HA chain was investigated by enzymatic cleavage of HA-C12 by SpHyl. The fraction of monosubstituted fragments is higher in water:1,4-dioxane (**Fig. 3**), while the fraction of bi- and trisubstituted oligomers is significantly higher in the water:tert-butanol mixture. This observation agrees with the MD simulations showing that in the water:tert-butanol solution the C_{12}-DMAP$^+$ ions are very hardly able to approach HA except for the close neighborhood of the already bound substituent. This preference is particularly strong at the substituent bound in the middle of the HA chain, a location dominating when longer chains are used. Therefore, the aliphatic sidechain probably serves as an entering gate for C_{12}-DMAP$^+$ in water:tert-butanol while in water:1,4-dioxane its influence on the subsequent substitutions is negligible.

5. Conclusions

The composition of mixed media of water and organic solvent have been shown to be a promising factor determining the efficiency of the mixed-anhydride based esterification reaction on hyaluronic acid and the evenness of the distribution of the substituents along the chain. In water:1,4-dioxane solution the substitution of HA by dodecanoyl residues provided higher degree of substitution as well as more even substituents distribution than in water:tert-butanol, both in the volume ratio 1:1. MD simulations of non-substituted and substituted HA molecules in the mixed solvents showed stronger water-enriched solvation shell of HA in water:tert-butanol forming a higher barrier for the approach of the reactant C_{12}-DMAP$^+$ to HA and thus causing a lower reaction rate in this solvent and even its rapid decrease at higher HA concentration in the reaction feed. However, an opposite solvent separation around the aliphatic chain enables the approach of C_{12}-DMAP$^+$ to HA in the proximity of an already bound substituent which may cause the clustering of substituents observed in water:tert-butanol. The MD results thus explain the experimental observations, consistent also with the previous study with oleoyl substituents [25], on the molecular level and open a way to the systematic investigation and utilization of the mixed solvents on the substitution reactions on polysaccharides.

Funding

The authors would like to thank the access to computing and storage facilities owned by parties and projects contributing to the National Grid Infrastructure MetaCentrum provided under the program "Projects of Large Research, Development, and Innovations Infrastructures" (CESNET LM2015042). This work was supported by the Ministry of

Education, Youth and Sports under the project „IT4 Innovations National Supercomputing Center – LM2015070“ and by the internal funding agency of Tomas Bata University in Zlin, no. IGA/FT/2016/011, IGA/FT/2017/009 and IGA/FT/2018/010. GHA has received funding from the Technology Agency of the Czech Republic: Program of Industrial Research and Experimental Development 2020-2027 (TREND), Project no. FW01010060.

References

[1] E. Fouissac, M. Milas, M. Rinaudo, R. Borsali, Influence of the ionic strength on the dimensions of sodium hyaluronate, Macromolecules. 25 (1992) 5613–5617. https://doi.org/10.1021/ma00047a009.

[2] K. Hayashi, K. Tsutsumi, F. Nakajima, T. Norisuye, A. Teramoto, Chain-stiffness and excluded-volume effects in solutions of sodium hyaluronate at high ionic strength, Macromolecules. 28 (1995) 3824–3830. https://doi.org/10.1021/ma00115a012.

[3] R. Mendichi, L. Soltés, A. Giacometti Schieroni, Evaluation of radius of gyration and intrinsic viscosity molar mass dependence and stiffness of hyaluronan, Biomacromolecules. 4 (2003) 1805–1810. https://doi.org/10.1021/bm0342178.

[4] M. Ingr, E. Kutálková, J. Hrnčiřík, Hyaluronan random coils in electrolyte solutions-a molecular dynamics study, Carbohydr. Polym. 170 (2017) 289–295. https://doi.org/10.1016/j.carbpol.2017.04.054.

[5] C.D. Blundell, P.L. DeAngelis, A. Almond, Hyaluronan: the absence of amide–carboxylate hydrogen bonds and the chain conformation in aqueous solution are incompatible with stable secondary and tertiary structure models, Biochem. J. 396 (2006) 487–498. https://doi.org/10.1042/BJ20060085.

[6] P. Gribbon, B.C. Heng, T.E. Hardingham, The analysis of intermolecular interactions in concentrated hyaluronan solutions suggest no evidence for chain-chain association., Biochem. J. 350 (2000) 329–335.

[7] J.E. Scott, F. Heatley, Hyaluronan forms specific stable tertiary structures in aqueous solution: A 13C NMR study, Proc. Natl. Acad. Sci. U. S. A. 96 (1999) 4850–4855. https://doi.org/10.1073/pnas.96.9.4850.

[8] J.E. Scott, F. Heatley, Biological Properties of Hyaluronan in Aqueous Solution Are Controlled and Sequestered by Reversible Tertiary Structures, Defined by NMR Spectroscopy, Biomacromolecules. 3 (2002) 547–553. https://doi.org/10.1021/bm010170j.

[9] E. Kutálková, J. Hrnčiřík, R. Witasek, M. Ingr, Effect of solvent and ions on the structure and dynamics of a hyaluronan molecule, Carbohydr. Polym. 234 (2020) 115919. https://doi.org/10.1016/j.carbpol.2020.115919.

[10] F. Bano, M.I. Tammi, D.W. Kang, E.N. Harris, R.P. Richter, Single-Molecule Unbinding Forces between the Polysaccharide Hyaluronan and Its Binding Proteins, Biophys. J. 114 (2018) 2910–2922. https://doi.org/10.1016/j.bpj.2018.05.014.

[11] F. Bongiovì, C. Fiorica, F.S. Palumbo, G. Di Prima, G. Giammona, G. Pitarresi, Imatinib-Loaded Micelles of Hyaluronic Acid Derivatives for Potential Treatment of

Neovascular Ocular Diseases, Mol. Pharm. 15 (2018) 5031–5045. https://doi.org/10.1021/acs.molpharmaceut.8b00620.
[12] G. Huerta-Ángeles, F. Ondreáš, M. Brandejsová, K. Kopecká, H. Vagnerová, J. Kulhánek, T. Drmota, Formulation of hyaluronan grafted with dodecanoic acid as a potential ophthalmic treatment, Carbohydr. Polym. 246 (2020) 116578. https://doi.org/10.1016/j.carbpol.2020.116578.
[13] G. Huang, H. Huang, Application of hyaluronic acid as carriers in drug delivery, Drug Deliv. 25 (2018) 766–772. https://doi.org/10.1080/10717544.2018.1450910.
[14] D. Šmejkalová, T. Muthný, K. Nešporová, M. Hermannová, E. Achbergerová, G. Huerta-Angeles, M. Svoboda, M. Čepa, V. Machalová, D. Luptáková, V. Velebný, Hyaluronan polymeric micelles for topical drug delivery, Carbohydr. Polym. 156 (2017) 86–96. https://doi.org/10.1016/j.carbpol.2016.09.013.
[15] A. Cadete, A. Olivera, M. Besev, P.K. Dhal, L. Gonçalves, A.J. Almeida, G. Bastiat, J.-P. Benoit, M. de la Fuente, M. Garcia-Fuentes, M.J. Alonso, D. Torres, Self-assembled hyaluronan nanocapsules for the intracellular delivery of anticancer drugs, Sci Rep. 9 (2019) 11565. https://doi.org/10.1038/s41598-019-47995-8.
[16] P. Walvekar, R. Gannimani, M. Salih, S. Makhathini, C. Mocktar, T. Govender, Self-assembled oleylamine grafted hyaluronic acid polymersomes for delivery of vancomycin against methicillin resistant Staphylococcus aureus (MRSA), Colloid Surf. B-Biointerfaces. 182 (2019) 110388. https://doi.org/10.1016/j.colsurfb.2019.110388.
[17] G. Huerta-Angeles, M. Brandejsová, R. Nigmatullin, K. Kopecká, H. Vágnerová, D. Šmejkalová, I. Roy, V. Velebný, Synthesis of graft copolymers based on hyaluronan and poly(3-hydroxyalkanoates), Carbohydr. Polym. 171 (2017) 220–228. https://doi.org/10.1016/j.carbpol.2017.05.011.
[18] X. Wang, J. Messman, J.W. Mays, D. Baskaran, Polypeptide grafted hyaluronan: synthesis and characterization, Biomacromolecules. 11 (2010) 2313–2320. https://doi.org/10.1021/bm1004146.
[19] S. Khetan, J.A. Burdick, Patterning network structure to spatially control cellular remodeling and stem cell fate within 3-dimensional hydrogels, Biomaterials. 31 (2010) 8228–8234. https://doi.org/10.1016/j.biomaterials.2010.07.035.
[20] E. Zerobin, M. Markovic, Z. Tomášiková, X.-H. Qin, D. Ret, P. Steinbauer, J. Kitzmüller, W. Steiger, P. Gruber, A. Ovsianikov, R. Liska, S. Baudis, Hyaluronic acid vinyl esters: A toolbox toward controlling mechanical properties of hydrogels for 3D microfabrication, J. Polym. Sci. 58 (2020) 1288–1298. https://doi.org/10.1002/pol.20200073.
[21] W.M. Payne, D. Svechkarev, A. Kyrychenko, A.M. Mohs, The role of hydrophobic modification on hyaluronic acid dynamics and self-assembly, Carbohydr. Polym. 182 (2018) 132–141. https://doi.org/10.1016/j.carbpol.2017.10.054.
[22] G. Huerta-Angeles, M. Bobek, E. Příkopová, D. Šmejkalová, V. Velebný, Novel synthetic method for the preparation of amphiphilic hyaluronan by means of aliphatic aromatic anhydrides, Carbohydr. Polym. 111 (2014) 883–891. https://doi.org/10.1016/j.carbpol.2014.05.035.
[23] Y. Xi, T. Jiang, Y. Yu, J. Yu, M. Xue, N. Xu, J. Wen, W. Wang, H. He, Y. Shen, D. Chen, X. Ye, T.J. Webster, Dual targeting curcumin loaded alendronate-hyaluronan-octadecanoic acid micelles for improving osteosarcoma therapy, Int. J. Nanomed. 14 (2019) 6425–6437. https://doi.org/10.2147/IJN.S211981.
[24] L. Vítková, L. Musilová, E. Achbergerová, A. Minařík, P. Smolka, E. Wrzecionko, A. Mráček, Electrospinning of Hyaluronan Using Polymer Coelectrospinning and Intermediate Solvent, Polymers. 11 (2019). https://doi.org/10.3390/polym11091517.

[25] O. Štrympl, J. Vohlídal, M. Hermannová, M. Maldonado-Domínguez, M. Brandejsová, K. Kopecká, V. Velebný, G. Huerta-Ángeles, Oleate-modified hyaluronan: Controlling the number and distribution of side chains by varying the reaction conditions, Carbohydr. Polym. 267 (2021) 118197. https://doi.org/10.1016/j.carbpol.2021.118197.
[26] S. Podzimek, M. Hermannova, H. Bilerova, Z. Bezakova, V. Velebny, Solution properties of hyaluronic acid and comparison of SEC-MALS-VIS data with off-line capillary viscometry, J. Appl. Polym. Sci. 116 (2010) 3013–3020. https://doi.org/10.1002/app.31834.
[27] D. Čožíková, T. Šílová, V. Moravcová, D. Šmejkalová, S. Pepeliaev, V. Velebný, M. Hermannová, Preparation and extensive characterization of hyaluronan with narrow molecular weight distribution, Carbohydr. Polym. 160 (2017) 134–142. https://doi.org/10.1016/j.carbpol.2016.12.045.
[28] J. Chmelař, A. Kotzianová, M. Hermannová, R. Šuláková, D. Šmejkalová, J. Kulhánek, V. Velebný, Evaluating the degree of substitution of water-insoluble acyl derivatives of hyaluronan using Raman spectroscopy: method development and comparison with gas chromatography and 1H NMR, Anal. Methods. 9 (2017) 232–239. https://doi.org/10.1039/C6AY03067J.
[29] J.C. Phillips, R. Braun, W. Wang, J. Gumbart, E. Tajkhorshid, E. Villa, C. Chipot, R.D. Skeel, L. Kalé, K. Schulten, Scalable Molecular Dynamics with NAMD, J. Comput. Chem. 26 (2005) 1781–1802. https://doi.org/10.1002/jcc.20289.
[30] O. Guvench, S.S. Mallajosyula, E.P. Raman, E. Hatcher, K. Vanommeslaeghe, T.J. Foster, F.W. Jamison, A.D. MacKerell, CHARMM Additive All-Atom Force Field for Carbohydrate Derivatives and Its Utility in Polysaccharide and Carbohydrate–Protein Modeling, J. Chem. Theory Comput. 7 (2011) 3162–3180. https://doi.org/10.1021/ct200328p.
[31] J.B. Klauda, R.M. Venable, J.A. Freites, J.W. O'Connor, D.J. Tobias, C. Mondragon-Ramirez, I. Vorobyov, A.D. MacKerell, R.W. Pastor, Update of the CHARMM All-Atom Additive Force Field for Lipids: Validation on Six Lipid Types, J. Phys. Chem. B. 114 (2010) 7830–7843. https://doi.org/10.1021/jp101759q.
[32] J. Lee, X. Cheng, J.M. Swails, M.S. Yeom, P.K. Eastman, J.A. Lemkul, S. Wei, J. Buckner, J.C. Jeong, Y. Qi, S. Jo, V.S. Pande, D.A. Case, C.L. Brooks, A.D. MacKerell, J.B. Klauda, W. Im, CHARMM-GUI Input Generator for NAMD, GROMACS, AMBER, OpenMM, and CHARMM/OpenMM Simulations Using the CHARMM36 Additive Force Field, J. Chem. Theory Comput. 12 (2016) 405–413. https://doi.org/10.1021/acs.jctc.5b00935.
[33] S.-J. Park, J. Lee, Y. Qi, N.R. Kern, H.S. Lee, S. Jo, I. Joung, K. Joo, J. Lee, W. Im, CHARMM-GUI Glycan Modeler for modeling and simulation of carbohydrates and glycoconjugates, Glycobiology. 29 (2019) 320–331. https://doi.org/10.1093/glycob/cwz003.
[34] W. Humphrey, A. Dalke, K. Schulten, VMD: visual molecular dynamics, J. Mol. Graph. 14 (1996) 33–38, 27–28.
[35] D. Šmejkalová, M. Hermannová, R. Šuláková, A. Průšová, J. Kučerík, V. Velebný, Structural and conformational differences of acylated hyaluronan modified in protic and aprotic solvent system, Carbohydr. Polym. 87 (2012) 1460–1466. https://doi.org/10.1016/j.carbpol.2011.09.057.
[36] J. Chmelař, J. Mrázek, M. Hermannová, L. Kubala, G. Ambrožová, A. Kocurková, T. Drmota, K. Nešporová, L. Grusová, V. Velebný, Biodegradable free-standing films from lauroyl derivatives of hyaluronan, Carbohydr. Polym. 224 (2019) 115162. https://doi.org/10.1016/j.carbpol.2019.115162.

[37] Y.K. Sung, S.W. Kim, Recent advances in polymeric drug delivery systems, Biomaterials Research. 24 (2020) 12. https://doi.org/10.1186/s40824-020-00190-7.
[38] D. Ret, G. Steiner, S. Gentilini, S. Knaus, Exact determination of the degree of substitution of high molar mass hyaluronan by controlling the conformation in solution, Carbohydr. Polym. 204 (2019) 124–130. https://doi.org/10.1016/j.carbpol.2018.10.003.
[39] S.D. Overduin, A. Perera, G.N. Patey, Structural behavior of aqueous t-butanol solutions from large-scale molecular dynamics simulations, J. Chem. Phys. 150 (2019) 184504. https://doi.org/10.1063/1.5097011.
[40] M.K. Cowman, T.A. Schmidt, P. Raghavan, A. Stecco, Viscoelastic Properties of Hyaluronan in Physiological Conditions, F1000Res. 4 (2015) 622. https://doi.org/10.12688/f1000research.6885.1.
[41] M. Cowman, S. Matsuoka, The intrinsic viscosity of hyaluronan, Hyaluronan. 1 (2002) 75–78. https://doi.org/10.1533/9781845693121.75.